

## Understanding the Mechanism of MgF<sub>2</sub> Modification on the Electrochemical Performance of Lithium-Rich Layered Oxides

Kai Yang<sup>1</sup>, Bangbang Niu<sup>2</sup>, Yanying Liu<sup>2</sup>, Jianjian Zhong<sup>2</sup> and Jianling Li<sup>2\*</sup>,

<sup>1</sup> China Electric Power Research Institute, Haidian District, Beijing 100192, China

<sup>2</sup> School of Metallurgical and Ecological Engineering, University of Science and Technology Beijing, No. 30 College Road, Haidian District, Beijing 100083, China

\*E-mail: [lijianling@ustb.edu.cn](mailto:lijianling@ustb.edu.cn)

Received: 9 November 2018 / Accepted: 27 December 2018 / Published: 10 March 2019

In this paper, lithium rich manganese based cathode materials were successfully modified by MgF<sub>2</sub> and the corresponding function mechanism was studied in detail. The MgF<sub>2</sub> coating inhibits the activation of Li<sub>2</sub>MnO<sub>3</sub> and induces the formation of spinel phase. The MgF<sub>2</sub>-3 shows an enhanced initial discharge capacity of 282.6 m Ah g<sup>-1</sup> and an improved coulombic efficiency of 87.15% compared to 267.8 m Ah g<sup>-1</sup> and 74.41% for the pristine sample, respectively. The MgF<sub>2</sub> modification can effectively inhibit HF corrosion, reduce side effects and improve cycle performance. The MgF<sub>2</sub>-3 shows a discharge capacity of 205.6 m Ah g<sup>-1</sup> with a retention of 80.03% and a voltage of 442.2mV after 200 cycles, while for the pristine is only 147.9 m Ah g<sup>-1</sup>, 66.71%, 672.3 mV, respectively.

**Keywords:** lithium rich cathode material, MgF<sub>2</sub> coating, cycling performance

### 1. INTRODUCTION

These years, the demand for high energy density lithium-ion batteries is gradually increasing and the cathode materials used commercially can't meet people's needs. Therefore, the search for a new generation of cathode materials has become the focus of research. In recent years, lithium-rich manganese-based cathode materials (LNCM) have attracted much attention due to their high capacity exceeding 250 m Ah g<sup>-1</sup>, and are expected to become the next generation of high-capacity cathode materials. Lithium-rich cathode materials are generally described as a composition of LiMO<sub>2</sub> and Li<sub>2</sub>MnO<sub>3</sub> [1]. The two phases are combined with each other crystallographically and can be described as a layered structure of O3. The high capacity of lithium-rich materials is due to their different charging and discharging mechanisms from ordinary cathode materials. For cathode materials, metal ions (Ni<sup>2+</sup>, Co<sup>3+</sup>) are oxidized during charging and lithium ions are released from the layered materials in the meantime. While for the lithium-rich materials, when the charging voltage over 4.45V, the lithium ions

will be released from  $\text{Li}_2\text{MnO}_3$  components and a special platform will appear in the charging curve [2-3]. Although lithium rich materials have very high discharge capacity, there are still many problems that limit their commercial application. Firstly, it will suffer great irreversible capacity loss in the first cycle due to the release of oxygen and Li in a form of  $\text{Li}_2\text{O}$  at the end of the first charging process [4]. Secondly, the poor performance at high rate due to its low electronic conductivity [5]. In addition, the vulnerable structure will suffer irreversible phase transformation and serious erosion, which lead to serious capacity loss and voltage decay.

In order to solve these problems, many researchers and scientists have done a lot of work, of which surface coating and bulk doping are two effective solutions. During electrochemical cycling process, even trace of water will cause the decomposition of electrolyte and generate HF, which will erode the surface of the material and affect the rate performance and cycle performance of the material. Surface coating with  $\text{Al}_2\text{O}_3$ [6],  $\text{CaF}_2$ [7],  $\text{AlF}_3$ [8] can effectively solve this problem. The coating layers act as a shield to protect the materials. Besides, In the process of material synthesis and electrochemical cycling, because the radius of  $\text{Ni}^{2+}$  and  $\text{Li}^+$  is similar, some  $\text{Li}^+$  and  $\text{Ni}^{2+}$  will be disordered, which affects the rate performance. During the electrochemical cycling, some cations will migration and leads to structural transformation which lead a bad effect on the cycle performance. Doping with special ions such as  $\text{Mg}^{2+}$  [9],  $\text{Y}^{3+}$  [10],  $\text{F}^-$  [11] can effectively reduce the  $\text{Li}^+/\text{Ni}^{2+}$  ions mixing and cations migration.

As we all know, the gradients do exist between the coating layer and the surface of cathode materials, which will lead ions diffusion in the process of material synthesis and electrochemical cycling. Therefore, seeking stable compounds composed of anions and cations with good doping properties as the coatings will combine the common advantages of bulk doping and surface coating, so that the properties of the materials will be improved. Among the doping ions,  $\text{Mg}^{2+}$  show good performance for its proper radiu, which is close to that of Li ion, and the inertia electrochemical property which has no effects on the electrochemical reactions. Anion  $\text{F}^-$  has strong electronegativity, which can effectively inhibit the migration of transition metals, reduce phase transition and stabilize the structure. It is generally believed that metal fluoride can effectively reduce the erosion of HF and improve the cycling performance of materials. Therefore, based on the above discussion, we contrive a novel design of surface coating with  $\text{MgF}_2$  for lithium-rich manganese-based materials. The experimental results show an improved first cycle efficiency, a better cycling performance and a reduced voltage decay for the  $\text{MgF}_2$  modified materials compared with the pristine. The reasons for improving electrochemical properties of materials by  $\text{MgF}_2$  coating will be further discussed in detail.

## 2. EXPERIMENTAL

### 2.1 Sample preparation

Lithium-rich manganese-based materials were synthesized by a co-precipitation method followed by high-temperature calcination. A mix solution of Manganese sulphate( $\text{MnSO}_4 \cdot \text{H}_2\text{O}$ ), cobalt sulphate( $\text{CoSO}_4 \cdot 7\text{H}_2\text{O}$ ), and nickel sulphate( $\text{NiSO}_4 \cdot 7\text{H}_2\text{O}$ ) (Mn: Co: Ni molar ration of 0.54: 0.13: 0.13 ) and a mixed solution of potassium hydroxide (KOH) and  $\text{NH}_3 \cdot \text{H}_2\text{O}$  were separately dropped into a continuously stirred reactor under the protection of  $\text{N}_2$  at  $60^\circ\text{C}$ . The pH value was maintained at 12

during the co-precipitation process. After the co-precipitation was completed, the precursor was cleaned and then dried at 120°C for 12 hours. The dried powder was then mixed with stoichiometric LiOH·H<sub>2</sub>O (5wt% excess) and preheated at 450°C for 5h then calcined at 900°C for 18 h in the air. After cooling to room temperature, the lithium- rich material was obtained. (marked as LNCM)

The MgF<sub>2</sub> modified lithium-rich manganese-based material was obtained by a chemical deposition method. First, the lithium-rich manganese-based material is dispersed in a mixed solution of ethanol and deionized (volume ratio of 1:1) water, and then a certain amount of Magnesium nitrate (Mg(NO<sub>3</sub>)<sub>2</sub>· 6H<sub>2</sub>O) is added and stirred uniformly. A certain amount of ammonium fluoride (NH<sub>4</sub>F) was dissolved in deionized water and stirred well. The ammonium fluoride solution was added dropwise to the previously obtained mixed solution, and heated and stirred at 80°C until evaporated. The MgF<sub>2</sub> (1wt%,3wt%,5wt%) modified lithium-rich manganese-based material was obtained after the evaporated powder was collected and calcined at 450°C for 5 hours.(marked as MgF<sub>2</sub>-1, MgF<sub>2</sub>-3, MgF<sub>2</sub>-5)

## 2.2 Material Characterization

The crystal structure of the material was characterized by X-ray diffraction with a 2θ range of 10-80°. Morphological studies on the samples were performed using a field emission scanning electron microscope (FESEM). The XPS measurement was performed to analyze the chemical state of the material elements and surface elements.

## 2.3 Electrochemical measurements

The electrode were fabricated from 75wt% of active material, 15wt% of super carbon black (Super-P) , and 10wt% of polypropylene difluoride(PVDF) and the cells were assembled in an Ar-filled glove box, Galvanostatic charge and discharge tests were performed between 2.0 and 4.8 V (vs. Li<sup>+</sup>/Li). The electrochemical impedance spectroscopy (EIS) of the coin cells were recorded in the charged state of 4.0 V at room temperature between 1 MHz and 10 mHz with an AC voltage of 5mV.

## 3. RESULTS AND DISCUSSION

In order to observe the morphology of each sample, SEM tests were carried out for each sample. As shown in **Fig. 1**, the precipitated particles in each sample are spherical particles with a diameter of about 200 nm. The surface of particles in **1-a** is smooth and clean, while a trace of precipitated particles is found on the surface of particles in **1-b**, which proves that MgF<sub>2</sub> has grown on the surface of particles. Figure **1-c** shows that there is an even coating layer on the surface of the particles, which indicates that MgF<sub>2</sub> grown well in situ. However, in **Fig. 1-d**, some scattered particles appeared on the surface of the spherical precipitated particles, which indicated that the amount of MgF<sub>2</sub> was too high and aggregated during in-situ growth. The results of SEM showed that MgF<sub>2</sub> was successfully grown on the surface of LNCM in situ during the wet chemical deposition process. Moreover, MgF<sub>2</sub>-3 show the best appearance and coating amount needed to be controlled reasonably.

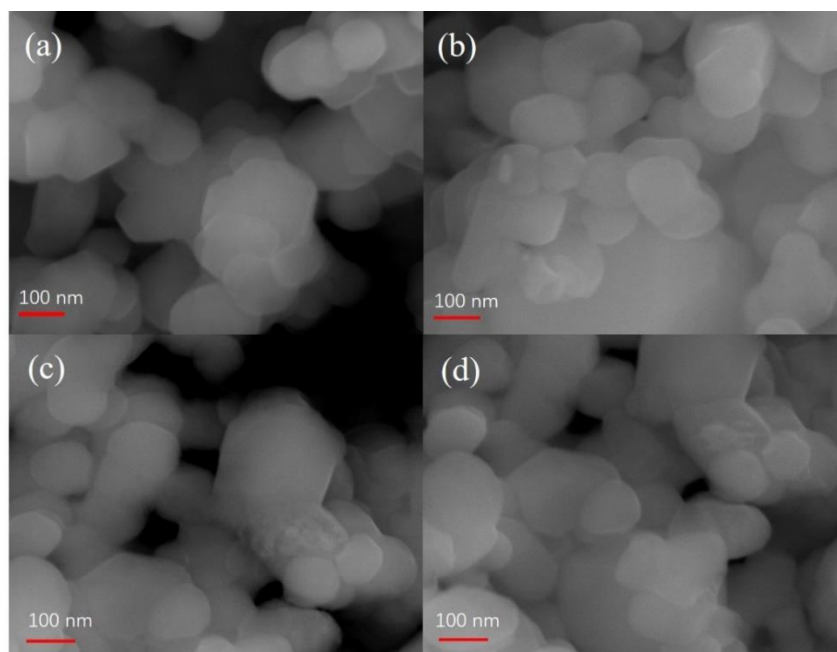


**Figure 1.** the SEM images of each sample (a) LNCM (b) MgF<sub>2</sub>-1 (c) MgF<sub>2</sub>-3 (d) MgF<sub>2</sub>-5

The crystal structure information of the four samples were characterized by power X-ray diffraction. **Fig. 2** shows the XRD spectra of the pristine and MgF<sub>2</sub> modified samples. It can be seen all the peaks appearing in the four samples can be perfectly indexed to a layered alpha -NaFeO<sub>2</sub> structure belonging to the R3m space group [12].

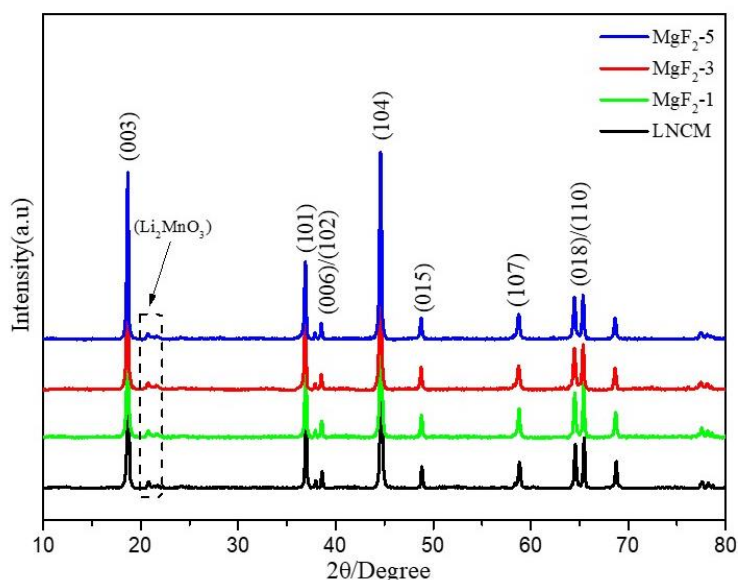


**Figure 2.** X-ray diffraction pattern of the LNCM, MgF<sub>2</sub>-1, MgF<sub>2</sub>-3, MgF<sub>2</sub>-5

Among them, the characteristic peaks near 20-25 degrees belong to the monoclinic Li<sub>2</sub>MnO<sub>3</sub> superlattice structure, which is caused by the intercalation of extra Li ions into the transition metal layers in the orderly lithium/transition metal layers. The peak splitting of (006)/(102) and (018)/(110) is obvious and the intensity is high, which indicates that each sample has an ordered layered structure [13]. However,

for the MgF<sub>2</sub> modified samples, we did not find the characteristic peaks of MgF<sub>2</sub>, which may be due their little amount. In order to further figure out the mechanism of MgF<sub>2</sub> modification, the lattice detail parameters of each sample were calculated by JADE6.0. As shown in the **Table. 1**

**Table 1.** The lattice parameters of four samples

	a	c	c/a
LNCM	2.84855	14.22183	4.99265
MgF <sub>2</sub> -1	2.86609	14.23072	4.96520
MgF <sub>2</sub> -3	2.85302	14.23658	4.98968
MgF <sub>2</sub> -5	2.85276	14.23644	4.99041

It can be seen from the table that both of the crystal parameters a and c increase after MgF<sub>2</sub> modification. According to the hexagonal crystal system, it is generally believed that the lattice parameter a imply the size of transition metal-oxygen slab and the lattice parameter c represents the interspacing of transition mental layers [14].

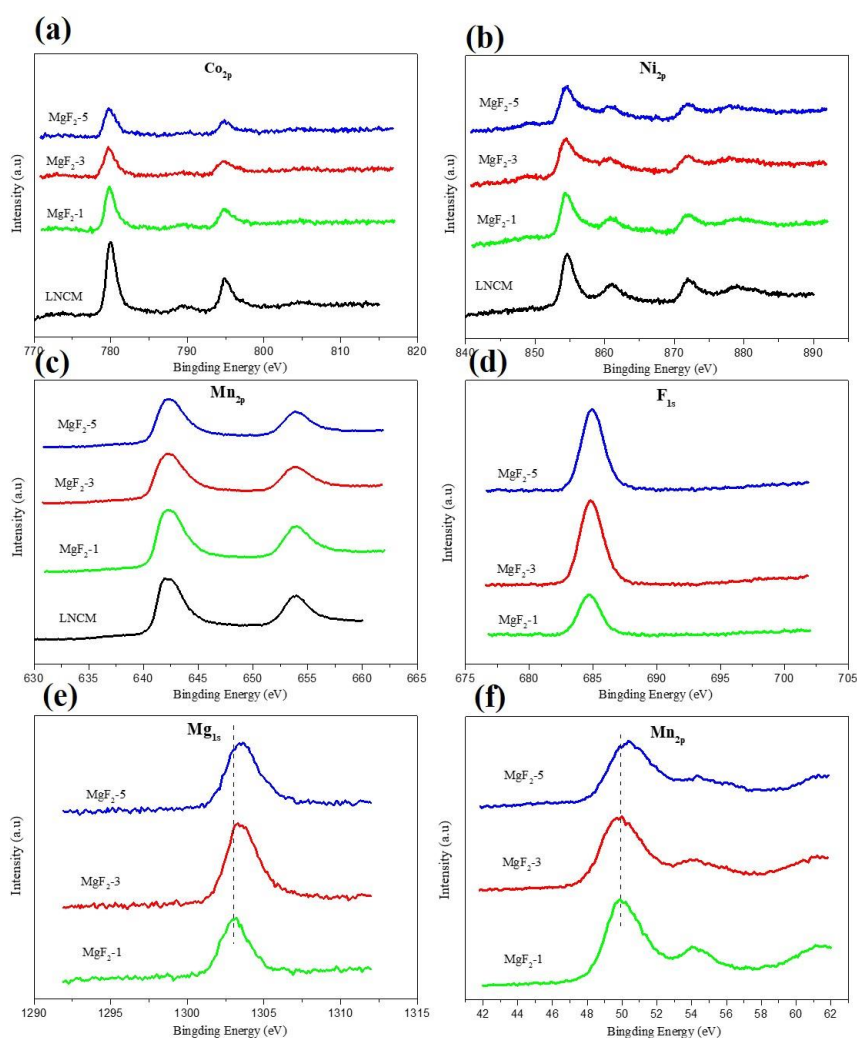


**Figure 3.** XPS spectra for (a)Ni<sub>2p</sub> (b)Mn<sub>2p</sub> (c)Co<sub>2p</sub> (d)F<sub>1s</sub>(e)Mg<sub>1s</sub>(f)Mn<sub>2p</sub>

This can be attributed to the fact that some  $\text{Mg}^{2+}$  and  $\text{F}^-$  may diffused into the inner of the material due to the gradient during the in-situ coating and the further calcination process. In the one hand, Mg has enlarged the lattice of the crystal structure, the can be due to the longer length of Mg - O bond than that of Ni - O bond [9]. On the other hand, some transition mental may be reduced to the lower chemical state because of  $\text{F}^-$  electronegativity and strong reducibility. The lower chemical state mental has the larger radius, which also leads to the increase of lattice crystal parameter a and c. Besides, the value of c/a for the four samples is lager than 4.9, which indicates all of them have an order structure.

In order to further analyze the chemical state of the material elements and surface elements, the XPS test for each sample were carried out. As shown in **Fig. 3**, the characteristic peals of  $\text{Ni}_{2p}$ ,  $\text{Co}_{2p}$ ,  $\text{Mn}_{2p}$  are all found in each sample, whose banding energy is 854.6eV, 779.7eV, 642.6eV [15], respectively, which is consistent with the reports. However, the characteristic peaks of Mg and F are only found in the modified samples, which indicates the  $\text{MgF}_2$  is successfully modified on the surface of the material. Moreover, the banding energy of  $\text{Mg}_{1s}$  and  $\text{Mg}_{2p}$  is 1304.95eV, 50.9eV, respectively. Careful observation found that the peaks of  $\text{Mg}_{1s}$  and  $\text{Mg}_{2p}$  gradually turns to the higher binding energy with the increase of coating amount. In order to figure out the mechanism, the detailed study was carried out in the fitting spectra for Mg. As shown in **Fig. 4**, Mg exist in two different chemical atmospheres after modification. One is bonding with F, the bond energy is 1303.9eV, the other is bonding with O, and the bond energy is 1303.9eV. This indicates that in the process of coating and subsequent calcination, some Mg from the coating layer diffuses into the bulk structure, replacing Ni and combining with O, which is consistent with the analysis of lattice parameters in XRD data.

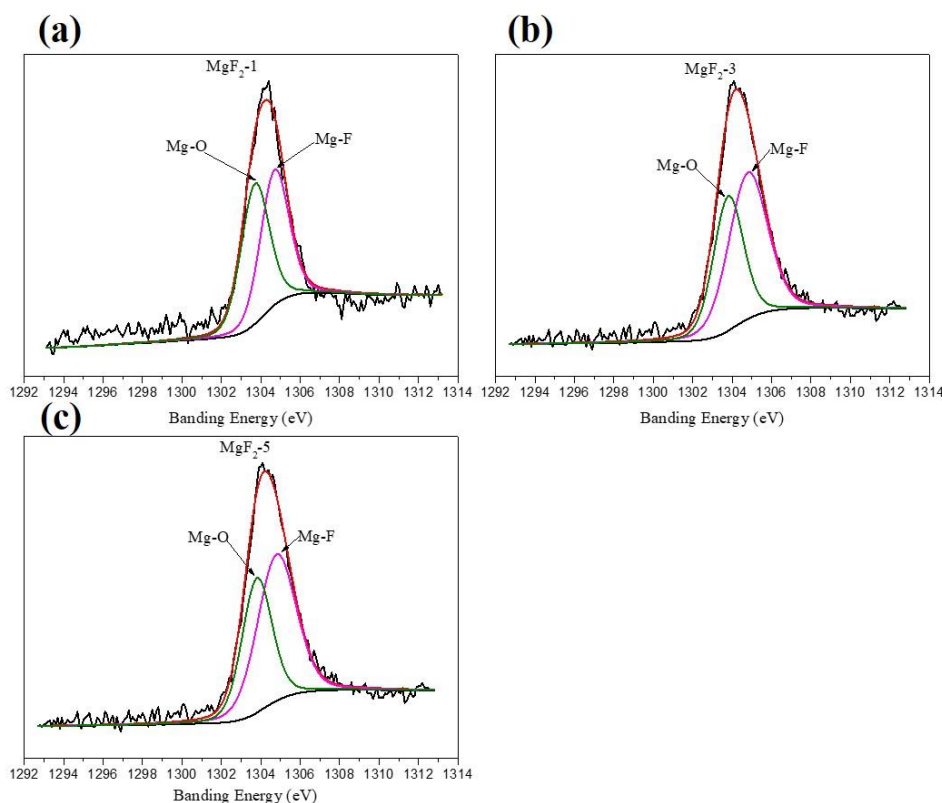


**Figure 4.** X-ray photoelectron spectrum of  $\text{MgF}_2$  modified samples.

**Fig. 5** shows the initial charge/discharge profiles(a) and the corresponding capacity differential curve(b) for each sample. It can be seen from **Fig. 2-a** that all the samples show a typical charging and discharging characteristics of lithium-rich materials, which consist of a slope and a platform about 4.45V [16]. During the slope part,  $\text{Li}^+$  separates from the interlayer of the solid solution phase  $\text{LiNi}_{1/3}\text{Co}_{1/3}\text{Mn}_{1/3}\text{O}_2$ . At the same time,  $\text{Li}^+$  in the octahedral voids of the  $\text{Li}_2\text{MnO}_3$  phase migrates to the interlayer tetrahedral voids, accompanied by the oxidation of transition metals  $\text{Ni}^{2+}/\text{Ni}^{3+}/\text{Ni}^{4+}$  and  $\text{Co}^{3+}/\text{Co}^{4+}$  [17]. It was found that the slope part shifted to the left after  $\text{MgF}_2$  modification, which indicates the charge capacity of this part decreased. This can be attributed to the fact that the relative content of active substances decreased after  $\text{MgF}_2$  coating. Between 4.4 V and 4.6 V, the voltage of the battery did not increase as the charging proceeded and show a long voltage plateau, corresponding to the strong oxidation peak near 4.5 V in the capacity differential curve [18]. Actually,  $\text{Li}^+$  continued to separate from  $\text{Li}_2\text{MnO}_3$  continuously with the increase of voltage after the oxidation process of  $\text{Ni}^{2+}/\text{Ni}^{3+}/\text{Ni}^{4+}$  and  $\text{Co}^{3+}/\text{Co}^{4+}$ , accompanied by the precipitation of  $\text{O}_2$ , which will interact with electrolyte and could not be completely embedded in solid solution phase, and finally  $\text{Li}^+$  was separated from  $\text{Li}_2\text{MnO}_3$  phase in the form of  $\text{Li}_2\text{O}$  [20]. The loss of oxygen vacancy in the bulk phase and  $\text{Li}^+$  partly returned to the solid solution phase eventually leads to the loss of capacity. Carefully observation find that the platforms were shortened after  $\text{MgF}_2$  modification, which indicates that  $\text{MgF}_2$  modification inhibited the activation of  $\text{Li}_2\text{MnO}_3$  and reduced the irreversible capacity loss. In addition, a small plateau appeared near 3.0V in the discharge curve of the modified samples, and a couple of 2.8V/3.2V redox peaks were found in the corresponding capacity differential curves. This is generally believed to be related to the insertion and extraction of  $\text{Li}^+$  ions at 16c octahedral sites of the spinel structure [21], which is contribute to improve the capacity. Therefore, after the modification of  $\text{MgF}_2$ , the charge capacity decreased from  $367.5 \text{ mAh g}^{-1}$  to  $324.3 \text{ mAh g}^{-1}$ , and the discharge capacity increased from  $267.8 \text{ mAh g}^{-1}$  to  $282.6 \text{ mAh g}^{-1}$ , and the initial coulombic efficiency increased from 74.41% to 87.15%.

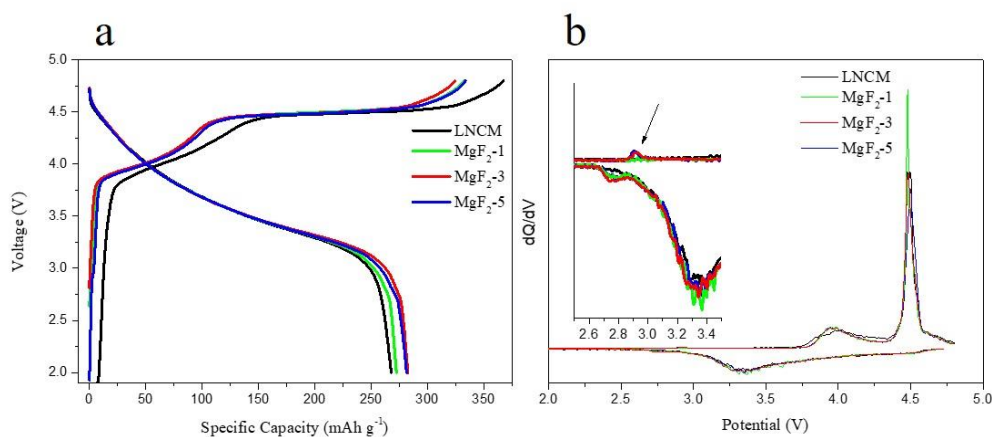


**Figure 5.** Initial cycle charge/discharge curves (a) and capacity differential curves (b) for each sample.

The rate performance of each sample is shown in **Fig. 6**. All the samples were charged/discharged at 0.05C during the first two cycles for activation, then charged at 0.1C, and discharged at 0.2C, 0.5C, 1C, 2C and 5C, respectively, and finally at 0.5C for the last 5 cycles. It can be seen from the profiles that the discharge capacity of each sample decreases with the rate increase. However, all the  $\text{MgF}_2$  modified

samples show the higher discharge capacity compared with the pristine at each rate. Specifically, the discharge capacity of MgF<sub>2</sub>-3 is 167.18 m Ah g<sup>-1</sup>, which is higher than 154 m Ah g<sup>-1</sup> for the pristine at 5C. The improvement of the rate performance can be attributed to the stable structure of MgF<sub>2</sub> coating layer, which reduce the side reactions and protect the surface of material from being eroded. On the other hand, a small amount of spinel phase formed during the coating process has a three-dimensional lithium ion diffusion channel, which also helps to improve the rate performance.

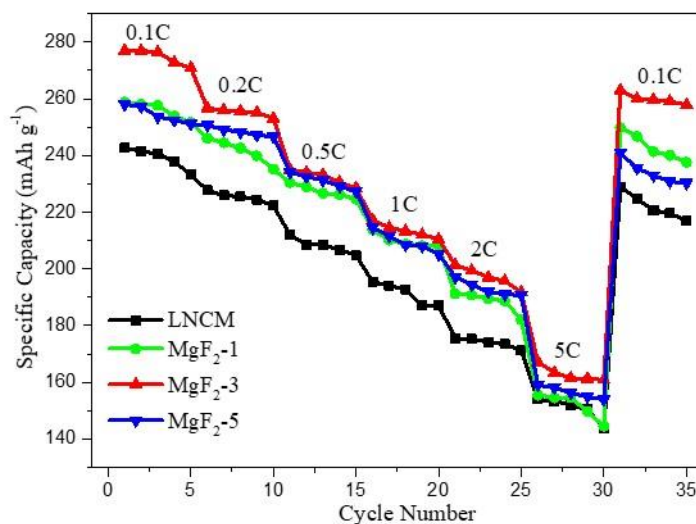


Figure 6. Rate performance of each sample

Table 2. Electrochemical Performance Comparison with other literature

Number	Caption	Initial Discharge Capacity at 0.05C	Rate Performance
1	This work	282.6 m Ah g <sup>-1</sup>	167.2 m Ah g <sup>-1</sup> at 5C
2	Reference 7	277.3 m Ah g <sup>-1</sup>	141.5 m Ah g <sup>-1</sup> at 3C
3	Reference 8	245.6 m Ah g <sup>-1</sup>	190 m Ah g <sup>-1</sup> at 2C
4	Reference 23	272 m Ah g <sup>-1</sup>	135 m Ah g <sup>-1</sup> at 5C

Table2 shows the comparison with similar lithium rich cathode materials which were described in literature. As can be seen from Table2, this work shows the highest initial discharge capacity and excellent rate performance among all the samples, which indicates that MgF<sub>2</sub> contributes to improve the electrochemical performance of LNCM.

Fig. 7 shows the cycling performance of the pristine and the modified samples. The samples were first activated at 0.05C for the first two cycles and then tested at 0.5C for 200 cycles. As can be seen from figure7-a, the cycling performance of the material has been significantly improved after MgF<sub>2</sub> modification. Specifically, the discharge capacity of MgF<sub>2</sub>-3 was 205.6 m Ah g<sup>-1</sup> and the retention rate was 80.03% after cycling for 200 cycles, while these of the pristine was only 147.9 m Ah g<sup>-1</sup> and 66.71%. Figure 7-b shows the voltage decay during the cycling process. It can be seen that the discharge voltage of all samples decreases with the cycle proceeding. However, the voltage drop is obviously reduced after

MgF<sub>2</sub> modification. Specifically, the voltage decay for MgF<sub>2</sub>-3 is 442.2mV after 200 cycles, which is lower than 672.3mV for that of the pristine. The voltage drop is obviously suppressed after modification by MgF<sub>2</sub>.

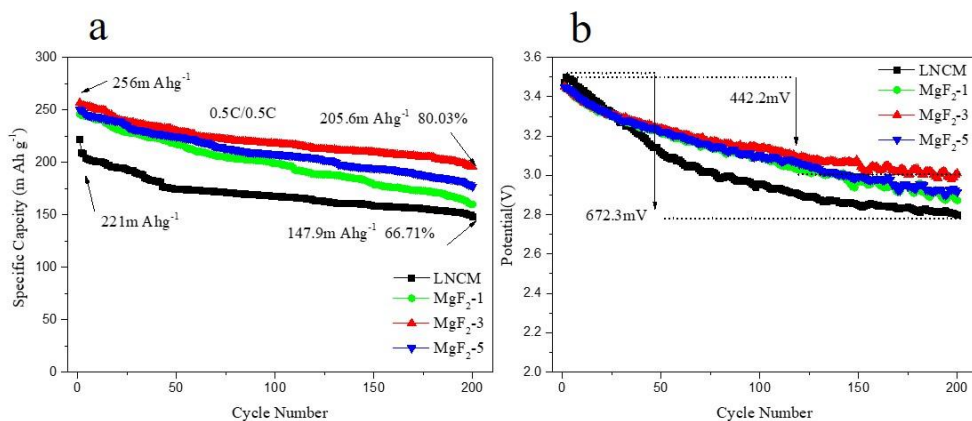


Figure 7. cycling capacity change curves (a) and voltage decay curves (b) for each sample.

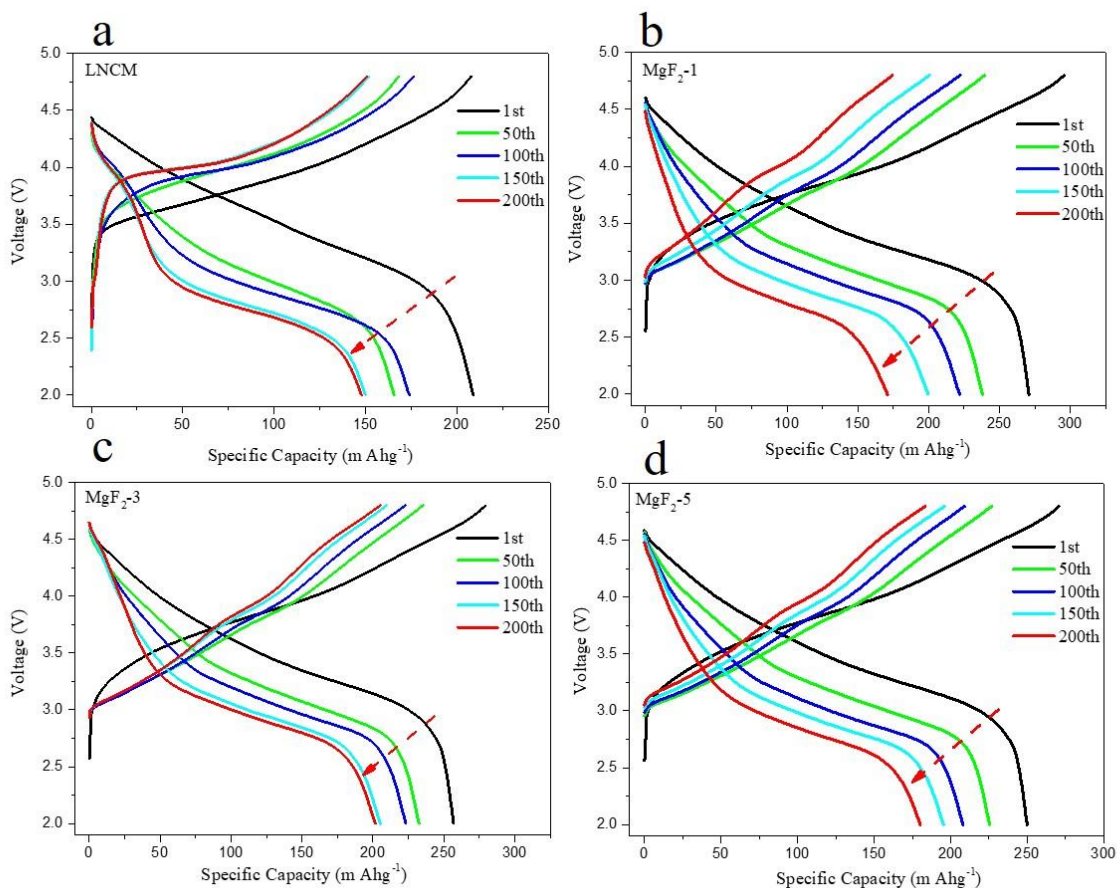
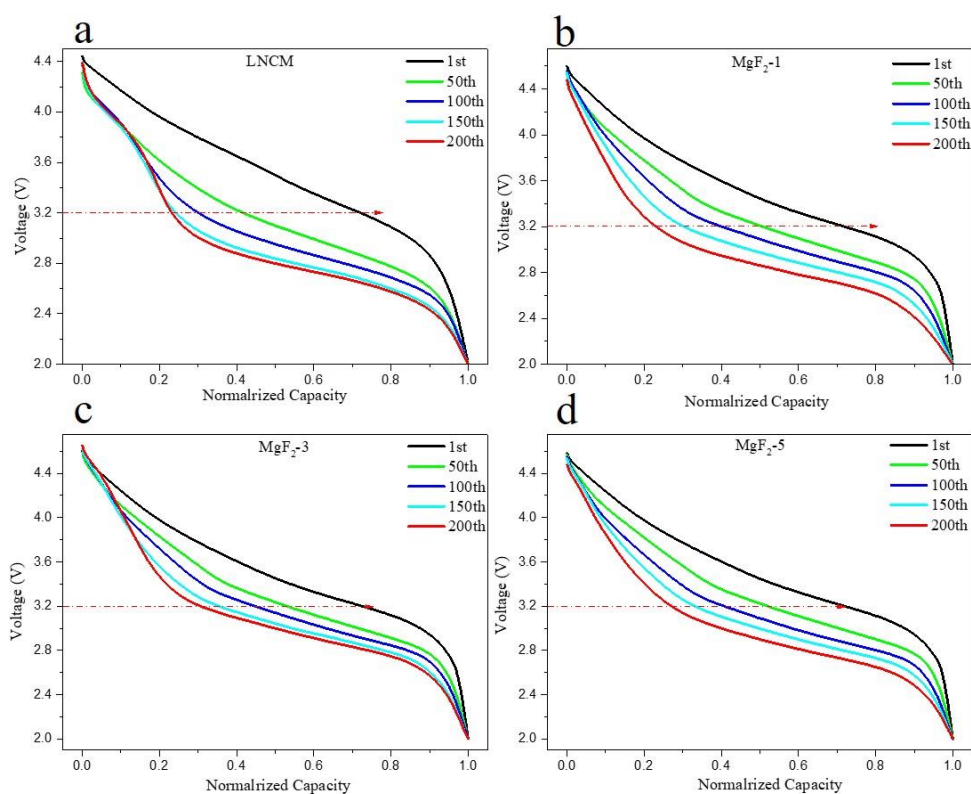


Figure 8. Cycling capacity curves of various samples (a) LNCM (b) MgF<sub>2</sub>-1 (c) MgF<sub>2</sub>-3 (d) MgF<sub>2</sub>-5

In order to further analyze the mechanism of capacity drop and voltage decay for each sample

during cycling, the charge/discharge curves of the 1st, 100th, 150th and 200th and the corresponding normalized discharge capacity curves were drawn. As shown in the **Fig. 8**, it can be seen that the charge/discharge capacity of the samples decreases gradually with the cycle proceeding. In particular, it can be seen that the discharge capacity curves of all the samples shrink internally near the discharge voltage of 3.2V. Further, **Fig. 9** shows the normalized discharge curves of the samples. It was found that the discharge capacity below 3.2V increased with the cycling, which corresponded to the decrease of discharge voltage during the cycling, while these decreases were reduced in the modified samples. It can be seen that about 80% of the discharge capacity for pristine comes from below 3.2V at 200th, while for that of MgF<sub>2</sub>-3 was 70%, which indicates that MgF<sub>2</sub> coating inhibits the capacity decay and voltage fading.



**Figure 9.** Normalized discharge capacity curve (a) LNCM (b) MgF<sub>2</sub>-1 (c) MgF<sub>2</sub>-3 (d) MgF<sub>2</sub>-5

Further, the capacity differential curves of each sample during the cycling was drawn. As shown in **Fig. 10**, in general, the capacity differential curve consists of three pairs of broad peaks, which are difficult to distinguish and correspond to the redox reactions of three transition metals. It can be seen that the cathodic reduction peak shifts to low voltage gradually with the cycle proceeding, but the shift of samples modified by MgF<sub>2</sub> slows down, which is consistent with the analysis of voltage drop curve and the normalized capacity curve. It is shown that the voltage fading of the materials is inhibited after MgF<sub>2</sub> modification. During the cycling process, the material structure gradually changes from layered to spinel phase. However, this kind of spinel phase formed in electrochemical process does not have the

characteristics of spinel phase, which will further transform into cubic salt rock facies [22]. The disordered salt-rock facies structure is electrochemically inert, and its lithium ion conductivity is very poor. The existence of a large number of salt-rock facies structure will cause serious capacity decay, voltage decline and polarization increase during the cycling process [23]. However, for the modified samples, the deviation of cathode peak and voltage drop were reduced, which indicates that the modified samples effectively inhibit the phase transition during the cycling process.

This can be attributed for two reasons. On the one hand, the  $\text{MgF}_2$  coating layer has an excellent stabilization effect, which can effectively reduce the erosion of HF and avoid the formation of surface corrosion pores. On the other hand, due to the gradient between the  $\text{MgF}_2$  coating layer and the material, some  $\text{Mg}^{2+}$  and  $\text{F}^-$  ions will diffuse into the bulk phase during the calcination process. The radius of  $\text{Mg}^{2+}$  ions is similar to that of  $\text{Li}^+$  ions, which can reduce the  $\text{Li}^+/\text{Ni}^{2+}$  mixing degree during the cycling process. Some  $\text{F}^-$  replaced  $\text{O}^{2-}$  and bound with transition metal. Because of the strong electronegativity of F, M-F bond is stronger and more stable than M-O bond, it can effectively inhibit the dissolution of transition metals and phase transition during charge/discharge process. Therefore, according to the above analysis, the cycling performance of the material has been greatly improved after  $\text{MgF}_2$  modification.

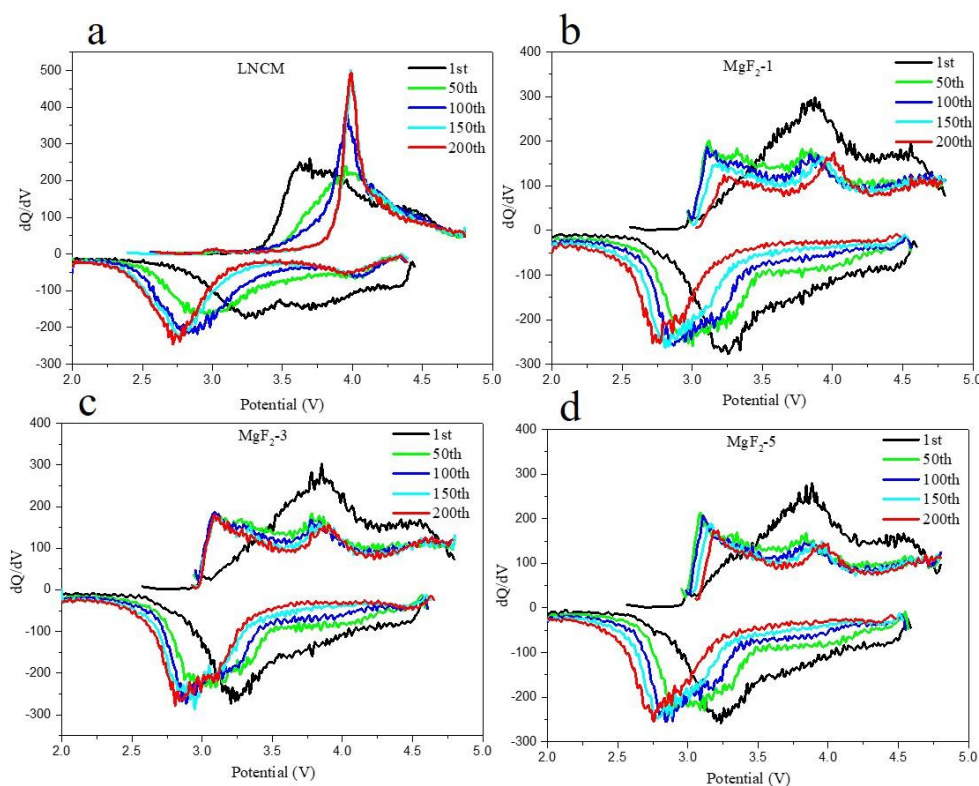


**Figure 10.** The capacity differential curves of each sample (a) LNCM (b)  $\text{MgF}_2$ -1 (c)  $\text{MgF}_2$ -3 (d)  $\text{MgF}_2$ -5

Electrochemical impedance spectroscopy (EIS) is often used to study the kinetics of electrochemical reaction of lithium ion batteries. In order to further explore the reasons for the improvement of the electrochemical properties of the materials before and after  $\text{MgF}_2$  modification, the

electrochemical impedance measurements were carried out after 100 cycles of each sample. The impedance spectra and the corresponding equivalent circuit diagrams of each material are shown in **Fig. 11**. Generally speaking, the electrochemical impedance spectrum of lithium ion battery is composed of two semicircles and a part of diagonal line [24]. The intercept between the high frequency half circle (the first half circle) and the real axis of the impedance spectrum represents the DC resistance, that is,  $R_s$  in the equivalent circuit, which is mainly caused by the electrolyte [25]. The semicircle of the high frequency part is the conduction impedance of lithium ion passing through the solid electrolyte membrane on the electrode surface, which is the  $R_{sf}$  in the equivalent circuit. The semicircle (the second semicircle) in the intermediate frequency area represents the charge conduction impedance [26], that is, the  $R_{ct}$  in the equivalent circuit. The Warburg impedance of lithium ion is shown by the oblique line in the low frequency region, that is,  $Z_w$  in the equivalent circuit.

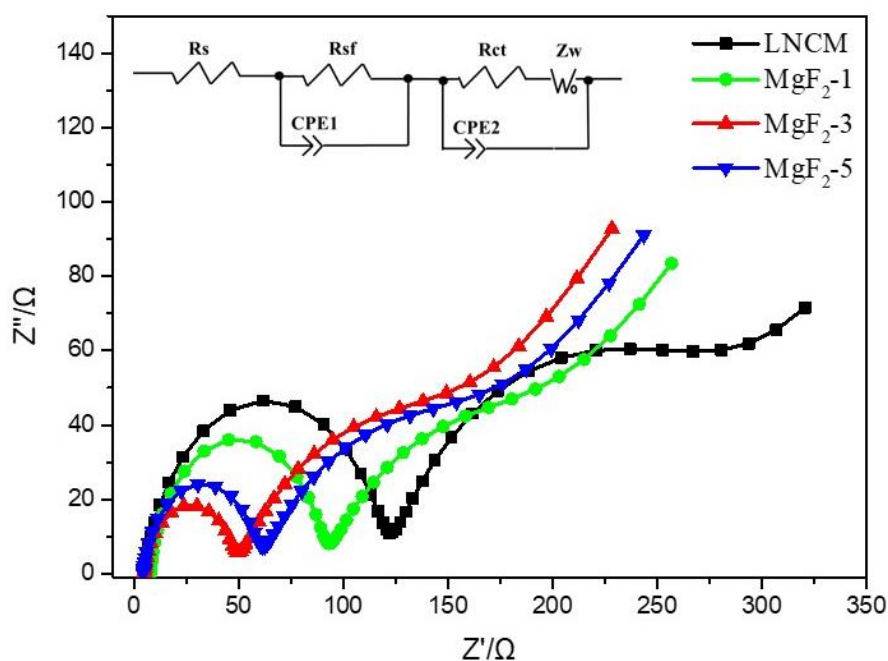


**Figure 11.** impedance spectrum and equivalent circuit diagram of each sample after 100 cycles.

**Table 3.** simulation impedance of equivalent circuit

R	LNCM	MgF <sub>2</sub> -1	MgF <sub>2</sub> -3	MgF <sub>2</sub> -5
$R_{sf}$ (Ω)	116.5	82.9	43.06	55
$R_{ct}$ (Ω)	173.6	125.9	100.5	129.9

According to the equivalent circuit diagram, the corresponding results were calculated and listed in **Table. 3**. After 100 cycles, the impedance values of each sample are composed of  $R_{sf}$  and  $R_{ct}$ . Among all the samples, the pristine material shows the largest the  $R_{sf}$ , which indicates that the material suffered serious corrosion during the cycling process [27]. After modification with MgF<sub>2</sub>, the impedance decreases continuously, which indicates that the MgF<sub>2</sub> coating layer can protect the surface of the

material from erosion. Specifically, when the modification amount is 1%, the impedance value decreases slightly, indicating the protective effect of MgF<sub>2</sub>. When the amount of MgF<sub>2</sub> rise to 3%, the modified material shows the lowest R<sub>sf</sub> value. While for the MgF<sub>2</sub>-5, the impedance value is slightly larger than MgF<sub>2</sub>-3, which may be due to the aggregation of the coatings. In addition, the R<sub>ct</sub> value of the initial material is the largest, indicating that the internal structure of the material changes after cycling, which is not conducive to the accumulation and dispersion of lithium ions. After MgF<sub>2</sub> modification, the R<sub>ct</sub> value decreases, which indicates that the structure of the material becomes more stable and the phase transition is inhibited [28]. Electrochemical impedance spectroscopy (EIS) analysis showed that the material had a more stable structure after MgF<sub>2</sub> modification, which was consistent with the previous electrochemical cycling analysis.

#### 4. CONCLUSIONS

In summary, the modification of lithium rich with MgF<sub>2</sub> was contrived by taking into account the advantages of surface coating and bulk doping. The MgF<sub>2</sub> coating layer were successfully modified on the surface of lithium-rich materials in situ by wet chemical deposition method. The experimental results show that MgF<sub>2</sub> has a good effect on improving the electrochemical properties of lithium-rich materials and the sample MgF<sub>2</sub>-3 shows the best performance. MgF<sub>2</sub> coating inhibits the activation of Li<sub>2</sub>MnO<sub>3</sub> thus reduces the irreversible capacity loss during the first cycle and improves the initial coulombic efficiency. Besides, the spinel phase formed during the coating process has a 3D lithium ion diffusion channel, which also helps to improve the rate performance. The stable MgF<sub>2</sub> coating effectively inhibits HF erosion, and the diffusion of some F-ions also plays a role in stabilizing the structure of the material. Therefore, the cycling performance of the material is improved and the voltage decay is reduced. The discussion of MgF<sub>2</sub> modification of Li-rich manganese-based materials should be helpful to find the new way to improve the performance of Li-rich manganese-based materials.

#### ACKNOWLEDGEMENTS

This work is financially supported by the National Natural Science Foundation of China (no. 51572024) and by the project of Research for Preparation and Modification of Li-rich Layered Cathode Materials (DG71-16-025).

#### References

1. F. Wu and G. Yushin, *Energy Environ. Sci.*, 10 (2017) 435.
2. J. Hong, H. Gwon, S.K. Jung, K. Ku and K. Kang, *J. Electrochem. Soc.*, 162 (2015) A2447.
3. J. Wang, X. He, E. Paillard, N. Laszczynski, J. Li and S. Passerini, (2016). *Adv. Energy Mater.*, 6 (2016) 1600906.
4. P.J. Phillips, J. Bareño, Y. Li, D.P. Abraham and R.F. Klie, *Adv. Energy Mater.*, 5 (2015) 1501252.
5. Y. Pei, Q. Chen, Y.C. Xiao, L. Liu, C. Xu, L. Zhen, G. Henkelman and G. Cao, *Nano Energy.*, 40 (2017) 566.

6. G. Kobayashi, Y. Irii, F. Matsumoto, A. Ito, Y. Ohsawa, S. Yamamoto, Y. Cui, J.Y. Son and Y. Sato, *J. Power Sources*, 303 (2016) 250.
7. X. Liu, J. Liu, T. Huang and A. Yu, *Electrochim. Acta*, 109 (2013) 52.
8. Y.K. Sun, M.J. Lee, C.S. Yoon, J. Hassoun, K. Amine and B. Scrosati, *Adv. Mater.*, 24 (2012) 1192.
9. Y. Wang, K. Shang, W. He, X. Ai, Y. Cao and H. Yang, *ACS Appl. Mater. Interfaces*, 7 (2015) 13014.
10. N. Li, R. An, Y. Su, F. Wu, L. Bao, L. Chen, Y. Zheng, H. Show and S. Chen, *J. Mater. Chem. A*, 1 (2013) 9760.
11. L. Li, B.H. Song, Y.L. Chang, H. Xia, J.R. Yang, K.S. Lee and L. Lu, *J. Power Sources*, 283 (2015) 162.
12. S.J. Shi, J.P. Tu, Y.Y. Tang, X.Y. Liu, Y.Q. Zhang, X.L. Wang and C.D. Gu, *Electrochim. Acta*, 88 (2013) 671.
13. C. Chen, T. Geng, C. Du, P. Zuo, X. Cheng, Y. Ma and G. Yin, *J. Power Sources*, 331 (2016) 91.
14. F. Ding, J. Li, F. Deng, G. Xu, Y. Liu, K. Yang and F. Kang, *ACS Appl. Mater. Interfaces*, 9 (2017) 27936.
15. P. Oh, M. Ko, S. Myeong, Y. Kim and J. Cho, *Adv. Energy Mater.*, 4 (2014) 1400631.
16. Y. Xie, M. Saubanere and M.L. Doublet, *Energy Environ Sci.*, 10 (2017), 266.
17. Z. He, Z. Wang, Z. Huang, H. Chen, X. Li and H. Guo, *J. Mater. Chem. A*, 3 (2015) 16817.
18. W.K. Pang, H.F. Lin, V.K. Peterson, C.Z. Lu, C.E. Liu, S.C. Liao and J.M. Chen, *Chem. Mater.*, 29 (2017) 10299.
19. Q. Xia, X. Zhao, M. Xu, Z. Ding, J. Liu, L. Chen, G.I. Douglas and W. Wei, *J. Mater. Chem. A*, 3 (2015) 3995.
20. Y. Zhao, J. Liu, S. Wang, R. Ji, Q. Xia, Z. Ding, W. Wei, Y. Liu, P. Wang and D.G. Ivey, *Adv. Funct. Mater.*, 26 (2016) 4760.
21. B. Li, C. Li, J. Cai and J. Zhao, *J. Mater. Chem. A*, 4 (2016) 14884.
22. F. Wu, N. Li, Y. Su, H. Lu, L. Zhang, R. An, Z. Wang, L. Bao and S. Chen, *J. Mater. Chem.*, 22 (2012) 1489.
23. X. Liu, Q. Su, C. Zhang, T. Huang and A. Yu, *ACS Sustainable Chem. Eng.*, 4 (2015) 255.
24. Y.F. Deng, S.X. Zhao, Y.H. Xu, K. Gao and C.W. Nan, *Chem. Mater.*, 27 (2015) 7734.
25. P. Oh, M. Ko, S. Myeong, Y. Kim and J. Cho, *Adv. Energy Mater.*, 4 (2014) 1400631.
26. R.P. Qing, J.L. Shi, D.D. Xiao, X.D. Zhang, Y.X. Yin, Y.B. Zhai, L. Gu and Y.G. Guo, *Adv. Energy Mater.*, 6 (2016) 1501914.
27. P.K. Nayak, J. Grinblat, M. Levi, E. Levi, S. Kim, J.W. Choi and D. Aurbach, *Adv. Energy Mater.*, 6 (2016) 1502398.
28. G. Kobayashi, Y. Irii, F. Matsumoto, A. Ito, Y. Ohsawa, S. Yamamoto, Y. Cui, J.Y. Son and Y. Sato, *J. Power Sources*, 303 (2016) 250.